

# Experimental and computational study of fracturing in an anisotropic brittle solid

Abbas Azhdari<sup>1</sup>, Sia Nemat-Nasser<sup>\*</sup>

*Center of Excellence for Advanced Materials, Department of Applied Mechanics and Engineering Sciences, University of California-San Diego, La Jolla, CA 92093-0416, USA*

Received 21 November 1996; revised 26 August 1997

## Abstract

For isotropic materials, stress- and energy-based fracture criteria lead to fairly similar results. Theoretical studies show that the crack-path predictions made by these criteria are not identical in the presence of strong material anisotropy. Therefore, experiments are performed to ascertain which criterion may apply to anisotropic materials. Notched specimens made from sapphire, a microscopically homogeneous and brittle solid, are used for the experiments. An attempt is made to locate the notch on different crystallographic planes and thus to examine the fracture path along different cleavage planes. The experimental observations are compared with the numerical results of the maximum tensile stress and the maximum energy-release rate criteria. It is observed that most of the notched specimens are fractured where the tensile stress is maximum, whereas the energy criterion fails to predict the fracture path of most of the specimens. For the tensile-stress fracture criterion, a dimensionless parameter,  $A^{(n)} = \sqrt{2\pi R_0} \sigma_{nn} / \sqrt{\gamma_\alpha E_{nn}}$ , is introduced, where  $\sigma_{nn}$  and  $E_{nn}$ , respectively, are the tensile stress and Young's modulus in the direction normal to the cleavage plane specified by the angle  $\alpha$  (the fracture surface energy of this plane is  $\gamma_\alpha$ ) and  $R_0$  is a characteristic length, e.g. the notch radius. Five out of six notched specimens which were tested, fractured at the point and along a cleavage plane where  $A^{(n)}$  is maximum. This parameter takes into account the effects of the surface energy of the corresponding cleavage plane, as well as the strength of the atomic bonds in the direction normal to the cleavage plane. It is suggested that for a specimen with a pre-existing crack, the maximum value of the parameter,  $A^{(c)} = K_{nn} / \sqrt{\gamma_\alpha E_{nn}}$ , should be used as the measure of the fracturing condition, where  $K_{nn}$  is the hoop stress intensity factor in the direction normal to the cleavage plane. For the notched sapphire specimens, Laue-diffraction analysis, along with the considerations of the geometry of the unit cell of sapphire, shows that the weakest family of cleavage planes,  $\{\bar{1}012\}$  and  $\{10\bar{1}0\}$ , are the fractured planes. © 1998 Elsevier Science Ltd. All rights reserved.

**Keywords:** Experimental fracture mechanics; Fracture criterion; Brittle fracture; Anisotropic; Sapphire; Hoop (normal) stress; Energy-release rate; Finite-element method

## 1. Introduction

For isotropic materials, fracture has been extensively studied both theoretically and experimentally,

whereas the analysis of cracks in anisotropic solids has received much less attention (for references, see Azhdari, 1995; Azhdari and Nemat-Nasser, 1996a,b). Under quasi-static loading, the often-used fracture criteria are: (1) maximum  $K_I$ , (2) zero  $K_{II}$ , (3) maximum hoop stress and (4) maximum energy-release rate. For isotropic cases, these criteria lead to

<sup>\*</sup> Corresponding author. E-mail: sia@ceam.ucsd.edu.

<sup>1</sup> E-mail: aazhdari@ceam.ucsd.edu.

fairly similar results. Theoretical studies, however, show that the crack-path predictions made by these criteria are not identical in the presence of anisotropy, e.g. each criterion predicts a different angle for the crack propagation from a pre-existing crack. There are other fracture criteria which stand on their own merit. Among these are the criteria of the strain–energy–density function (Sih, 1972), the normal-stress ratio (Buczek and Herakovich, 1985) and the tensor polynomial (Tsai and Wu, 1971; Wu, 1974). The last two fracture criteria have been proposed to assess the fracture resistance of structures fabricated from composite materials. The inconsistency in the predictions of various fracture criteria is demonstrated by, e.g. Obata et al. (1989), Azhdari (1995) and Azhdari and Nemat-Nasser (1996a,b), where additional references are also found. Fracture criteria should be based upon physical models and experimental observations, established from the knowledge of the fracturing mechanisms. Therefore, experiments should be performed to ascertain which criterion is applicable to anisotropic materials, e.g. when fracture occurs and in which direction it propagates. In addition, if none of the existing criteria can predict the fracture, then other alternatives must be sought, based on theoretical and experimental studies. The experimental work reported here is a step in this direction.

Theoretical studies have focused on homogeneous anisotropic materials. Highly heterogeneous composite materials tend to complicate the experimental results. Although each constituent of a composite material (e.g. matrix, fibers, whiskers) may be considered separately as a homogeneous material, the composite itself is inhomogeneous at a length-scale which is large enough to complicate the fracture process. A class of materials which can be used for our purposes is that of single crystals which are microscopically homogeneous and anisotropic. In the process of material selection, in addition to being single-crystal, material brittleness is also important; in ductile materials a plastic region is invariably formed around the crack tip. In addition to the homogeneity and brittleness, it is preferable to perform the experiments on thin plates, since theoretical studies often consider plane problems (plane stress or plane strain). This provides closer connection between the theoretical work and the experiments. In

view of the above considerations and also of material availability, *sapphire* was chosen for our experiments.

The crystallographic structure of sapphire is hexagonal–rhombohedral. Its unit cell is shown in Fig. 1. In a single crystal, different crystallographic planes have different surface energies which have an important influence on the fracture process. For alumina (polycrystalline sapphire), the tensile strength is approximately 0.20 GPa, while the tensile strength of sapphire is 7–15 GPa which is fairly close to the theoretical strength. Because of the very high surface energy of the (0001)-plane, the fracture of sapphire usually does not occur along the basal plane. Separation along this plane is very difficult because it is not electrostatically neutral. The unit cell can be visualized as aluminum ions stacked between the basal planes of oxygen atoms. Thus, the creation of a fracture surface on the basal plane, (0001), would

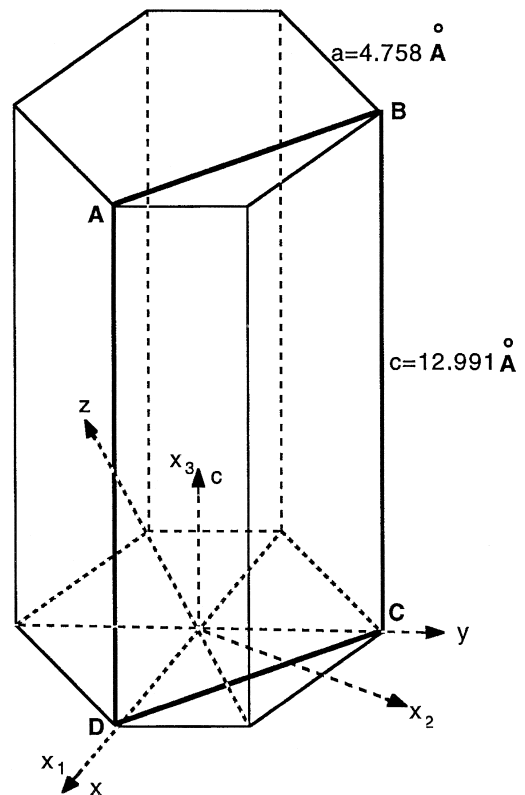


Fig. 1. Coordinate systems in the crystallographic structure of sapphire; ABCD is the (11 $\bar{2}$ 0)-plane (coordinate systems are not related to those shown in Figs. 2, 3, 5, 6, 7, and 8).

Table 1  
Fracture surface energies of different cleavage planes in sapphire

Fracture plane	(0001)	$\{\bar{1}\bar{1}26\}$	$\{10\bar{1}0\}$	$\{\bar{1}012\}$
Energy (J/m <sup>2</sup> )	> 40	24.4	7.3	6

necessitate the separation between planes of oppositely charged ions and would require a great deal of energy. Wiederhorn (1969) has measured the surface energies for sapphire along some crystallographic planes using the double-cantilever technique which was originally devised by Gilman (1960); see Table 1 for fracture surface energies of the cleavage planes (0001),  $\{\bar{1}\bar{1}26\}$ ,  $\{10\bar{1}0\}$  and  $\{\bar{1}012\}$ . Table 1 shows that the  $\{10\bar{1}0\}$ - and  $\{\bar{1}012\}$ -planes would be preferred planes for fracturing. These relatively high values of the surface energy also explain why fracture in polycrystals tends to be intergranular.

Experiments are performed on notched sapphire specimens. An attempt has been made to locate the notch on different crystallographic planes (see Table 1) and, thus, to examine the fracture path along different cleavage planes. In order to support and verify the experimental results, the finite-element code ABAQUS is used to analyze the stress field in the samples. This code is capable of handling elasticity problems with any degree of anisotropy. The calculation of the material constants of sapphire, finite element method (FEM) pre-processing and FEM simulation are presented. Then the post-processing of the FEM results and a discussion are given. The experimental observations are compared with the results of the maximum-tensile-stress and maximum-energy-release-rate fracture criteria, calculated by FEM. The results are compared and discussed. Finally, a summary and then the conclusions are given.

## 2. Experimental procedure

### 2.1. Material selection (sapphire)

Sapphire, the single-crystal alumina (Al<sub>2</sub>O<sub>3</sub>), which is very brittle and has a high modulus, was chosen for the experiments. Sapphire plates with the (11 $\bar{2}$ 0)-orientation and 127 × 127 × 2 mm size (127 mm = 5 inch) were used. This crystallographic plane is shown in Figs. 1 and 2 as the rectangle ABCD.

Saphikon (located in Milford, New Hampshire) has supplied the sapphire sheets. According to this company’s catalog, some of the physical/mechanical properties of sapphire are as follows:

Crystallographic structure: Hexagonal, rhombohedral single crystal

Tensile strength: 60,000 psi (at 25°C)

Compressive strength: 350,000 psi

Young’s modulus: 60 × 10<sup>6</sup> psi (414 GPa) (at 25°C)

Poisson’s ratio: 0.28–0.33

Hardness: 9 on MOHS scale (quartz is 7, diamond is 10)

Melting point: 2,053°C

We establish the intersection of the as-received sapphire sheet with the cleavage planes recorded in Table 1. The intersection of this sheet with the four crystallographic planes (0001),  $\{\bar{1}\bar{1}26\}$ ,  $\{10\bar{1}0\}$  and  $\{\bar{1}012\}$ , can be found by considering the geometry of the unit cell (Fig. 1). The six lines of intersection are shown in Fig. 2, which displays the directions on the (11 $\bar{2}$ 0)-plane in which fracture would possibly occur. For example, considering Table 1, the horizontal line in Fig. 2 has the minimum chance of being the

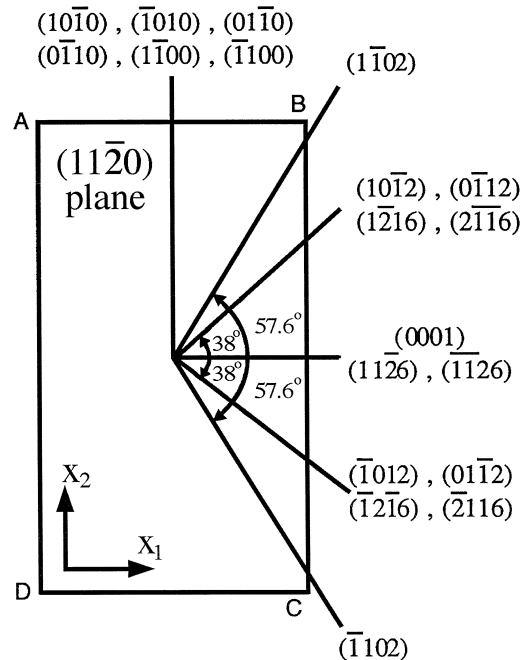


Fig. 2. Intersection of (11 $\bar{2}$ 0)-plane with other cleavage planes of sapphire.

fracture direction because this line is the intersection of the strongest plane, the (0001)-plane, with the sapphire sheet. All the other lines in Fig. 2 are potential fracture directions, depending upon the loading direction, geometry, etc. Fig. 2 is a key for the specimen design, showing the direction in which the specimen should be cut out from the as-received sapphire sheet.

### 2.2. Specimen design

The ultimate goal of this study is to examine the kinking direction of a pre-existing crack in an

anisotropic solid. However, in highly brittle materials such as sapphire, it is very difficult to extend an existing crack in a stable manner and arrest it. Therefore, the simpler case of a sample with a pre-existing notch (instead of a crack) is considered.

Specimens of the size of  $24 \times 24 \times 2$  mm are used. A semi-circular notch with a radius of 2 mm is produced on one side of the specimen. At first glance, a 2 mm notch may seem too wide to simulate a crack, but as will be shown later, when the notch radius is large, points on the notch surface are more distinguishable for measurement. As a result, the

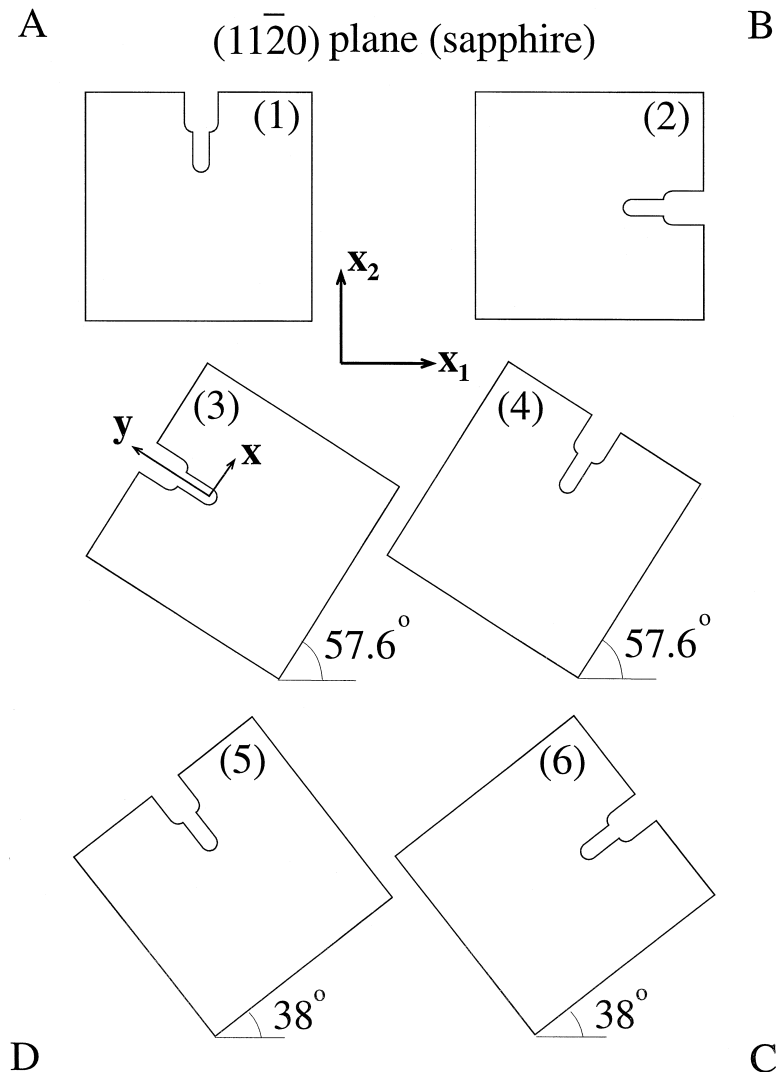


Fig. 3. Notched specimens of different orientations are obtained from the as-received sapphire sheet.

fracture-initiation point may be measured more accurately. Location of the fracture initiation point is a prime parameter in the tests (see the results and discussion in Section 5).

For each specimen, the direction of the notch aligns with one of the six lines shown in Fig. 2. As a result, different specimens have different crystallographic directions in the same crystallographic plane. Fig. 3 shows how the six specimens and their corresponding notches relate to the as-received sapphire sheet. Each specimen makes some angle,  $\theta$ , with respect to the coordinate system of the sheet ( $\theta$  is the angle between the  $x_1$ - and  $x$ -directions, measured counterclockwise). The procedure to calculate the elastic–stiffness constants with respect to the specimen coordinate system ( $x$ – $y$  system in Fig. 3) is presented in Section 3.1.

### 2.3. Loading device

Due to the brittleness and hardness, machining and drilling of sapphire are difficult. For example, making a compact-tension specimen requires drilling two holes in the specimen, which is relatively difficult. Secondly, a displacement-controlled test is desirable because it provides stable crack growth. For a highly brittle material such as sapphire, the energy required for crack extension is relatively small. Therefore, once a crack is initiated, it may continue to propagate even under the (nominally) displacement-controlled conditions. Specimens are therefore designed such that they can be made with minimal machining and they are loaded by a displacement-controlled mechanism.

The loading device uses the thermal expansion of a small block of steel ( $4 \times 4 \times 10$  mm); see Fig. 4. The steel block with a thermal-expansion coefficient of  $20 \times 10^{-6}/^\circ\text{C}$  is fitted inside the notch, and then heated by a soldering iron. The effective length of the block of steel is about 4 mm. It is observed that the specimens are fractured when the steel block reaches a temperature of around 150 to 200°C. The objective of the test is to measure the point on the notch surface at which the fracture is initiated and, also, to determine which cleavage plane is the fractured plane. Due to the linearity of the system, the magnitude of the load exerted by the steel block on

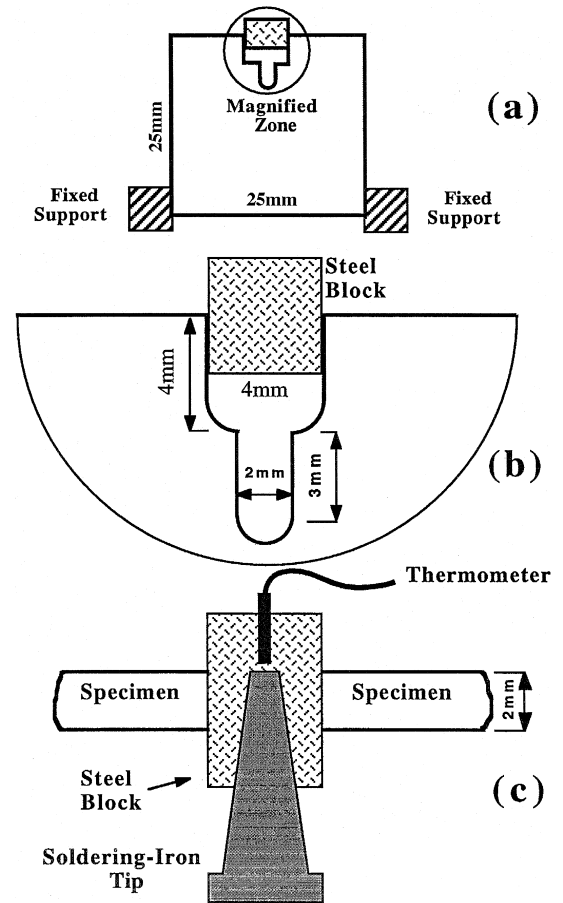


Fig. 4. (a) Overall view of specimen setup, (b) magnified front view and (c) magnified top view.

the specimen does not affect these quantities; see Sections 3 and 4.

## 3. FEM simulation

### 3.1. Calculation of elastic–stiffness matrix

No closed-form solution exists for anisotropic notched specimens of finite size. Therefore, comparison of the experimental and theoretical results requires a numerical approach using, for example, a finite-element method. The commercial FEM code, ABAQUS which can handle elasticity problems of any degree of anisotropy is used. In general, any FEM code requires that the input elastic–stiffness

matrix be expressed with respect to the body-coordinate system (e.g. the  $x$ - $y$  coordinate system in Fig. 3). The stress-strain relation for a generally anisotropic linearly elastic body,  $\sigma_{ij} = s_{ijmn} \epsilon_{mn}$  ( $i, j, m, n = 1, 2, 3$ ), is expressed in matrix notation as  $\{\tau\} = [S]\{\gamma\}$  or  $\{\gamma\} = [C]\{\tau\}$ , where  $[C] = [S]^{-1}$ ; the vectors  $\tau$  and  $\gamma$  are the compact forms of the stress and strain (engineering) tensors and  $S$  and  $C$  are the stiffness and compliance matrices, respectively. Energy and symmetry considerations reduce the number of elastic constants to 21. Fig. 1 shows the rectangular Cartesian coordinate system,  $x_1$ - $x_2$ - $x_3$ , to which the elastic constants are referred, and the hexagonal coordinate system,  $x$ - $y$ - $z$ - $c$ , which is

used for the Miller-Bravais indices. For sapphire, the symmetry of point group  $\bar{3}m$  reduces the number of independent elastic stiffness (or compliance) constants from 21 to 6. For example, the elements of the elastic-stiffness matrix for sapphire, referred to the coordinate system  $x_1$ - $x_2$ - $x_3$ , of Fig. 1, reported by Wachtman et al. (1960), are:

$$S_{11} = 4.968, S_{12} = 1.636, S_{13} = 1.109, S_{14} = 0.235,$$

$$S_{15} = 0, S_{16} = 0, S_{22} = S_{11}, S_{23} = S_{13},$$

$$S_{24} = -S_{14}, S_{25} = 0, S_{26} = 0, S_{33} = 4.981,$$

$$S_{34} = 0, S_{35} = 0, S_{36} = 0, S_{44} = 1.474, S_{45} = 0,$$

$$S_{46} = 0, S_{55} = S_{44}, S_{56} = S_{14}, S_{66} = (S_{11} - S_{22})/2.$$

Note that the units are  $10^{-12}$  dyn/cm<sup>2</sup> where 1

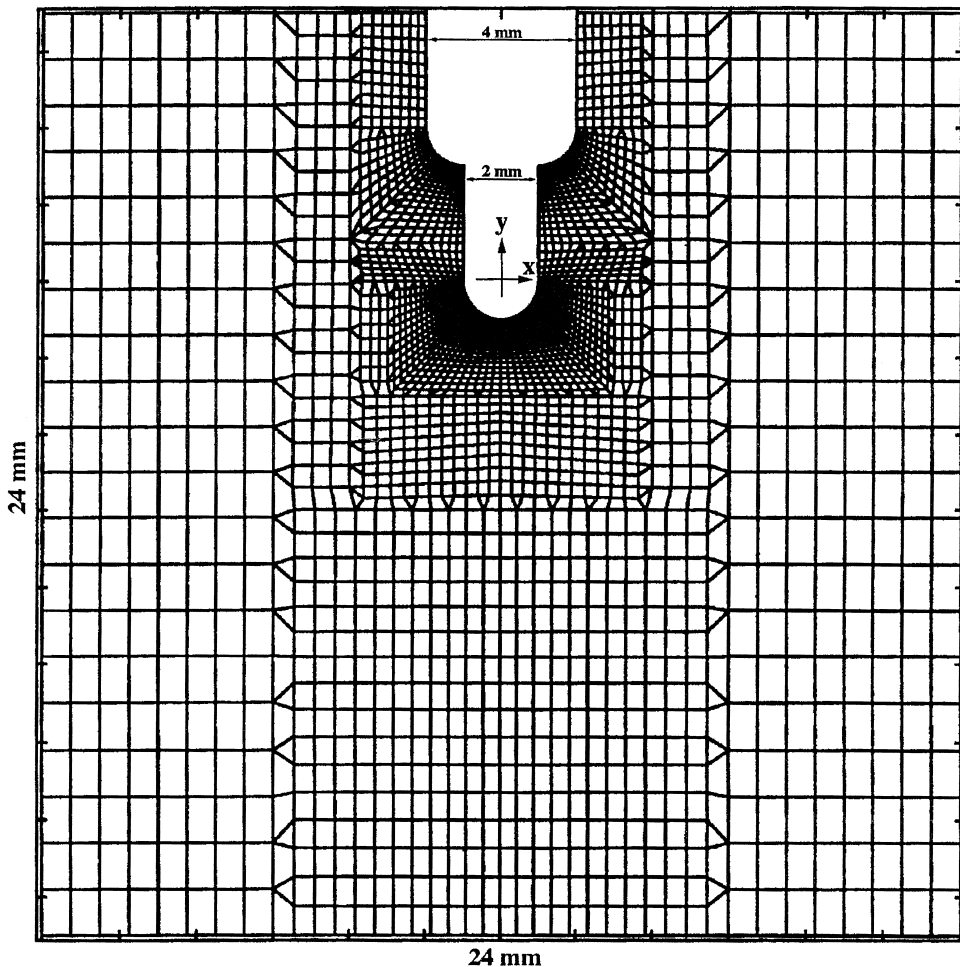


Fig. 5. FEM mesh for the notched specimen (2984 elements and 3047 nodes).

dyn/cm<sup>2</sup> = 14.503 × 10<sup>-6</sup> psi, e.g.  $S_{11} = 4.968 \times 10^{12}$  dyn/cm<sup>2</sup> = 72.05 × 10<sup>6</sup> psi.

As mentioned earlier, the experiments are performed on samples obtained from a (11 $\bar{2}$ 0)-sapphire plate. For FEM calculations, the elastic-stiffness matrix,  $s'_{ijkl}$ , in the (11 $\bar{2}$ 0)-plane ( $x$ - $y$  coordinate system in Fig. 3) is required. This is given by  $s'_{ijkl} = R_{im}R_{jn}R_{kp}R_{lq}s_{mnpq}$ , where  $R_{ij}$  is the corresponding orthogonal rotation tensor which transforms the components of an arbitrary vector given in the unprimed system ( $x_1$ - $x_2$ - $x_3$  in Fig. 1) to the

components of the same vector given in the primed system (e.g.  $x$ - $y$  in Fig. 3); see Azhdari (1995) for more details.

### 3.2. Mesh generation and external loading simulation

Finite-element calculations are performed using 2984 elements and 3047 nodes (Fig. 5). Note that this mesh considers 48 nodes on the inner surface of the notch, and thus the numerical investigation in regard to the stresses on the notch surface is per-

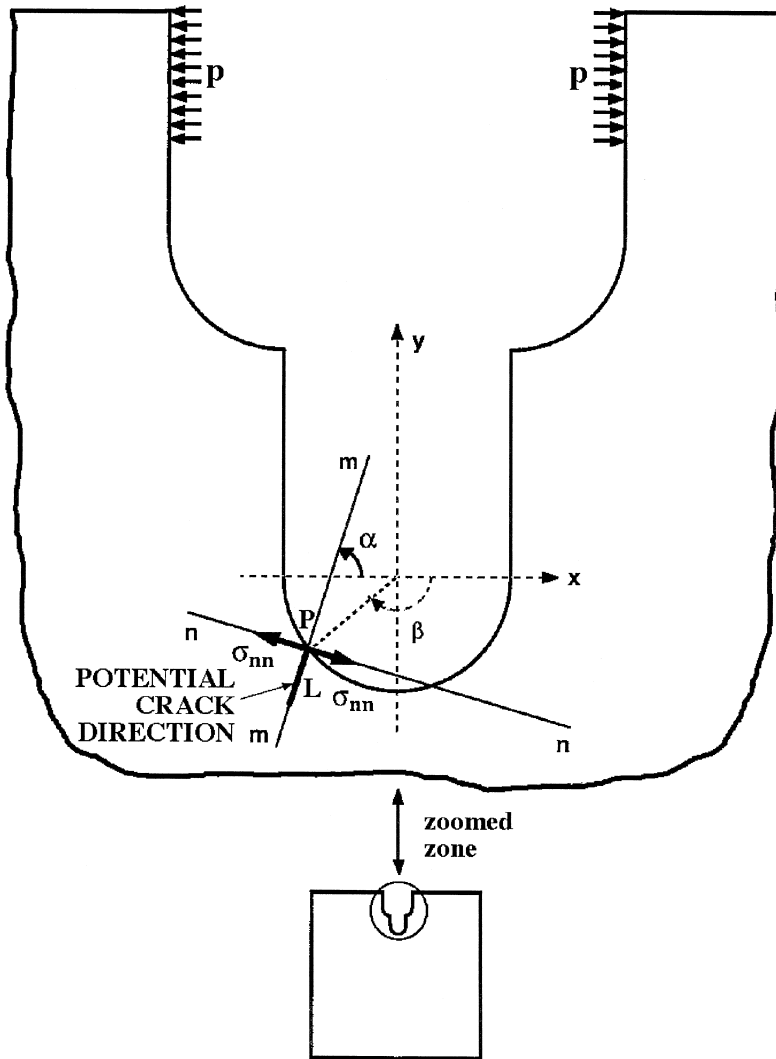


Fig. 6. Tensile stress  $\sigma_{nn}$  acting normal to the cleavage plane  $m$ - $m$  at an arbitrary point  $P$ , creating a crack of length  $L$ .

formed at just these 48 distinct nodes. Uniform pressure  $p$  (Fig. 6) is assumed to act on the contact area between the steel block and the specimen as shown in Fig. 6. The magnitude of this uniform pressure is not needed if just the location and the orientation of the planes which carry the maximum tensile stresses are of interest (this is because the behavior of the system is assumed to be linear, i.e. the response of the system is proportional to  $p$ ). Thus, no effort was made to measure the magnitude of the applied pressure. Finally, a plane-stress condition is assumed which is suitable for the thin specimens used. FEM is used to calculate the *tensile stresses* acting on the inner surface of the notch, and also to estimate the *energy-release rate* for possible cracking along different crystallographic planes on the notch surface.

## 4. FEM results

### 4.1. Calculation of the stress field near the notch surface

Under the conditions described in Section 3.2, the displacement and stress fields are calculated for each specimen shown in Fig. 3, using the FEM code ABAQUS. Since the stress concentration is relatively high on the inner surface of the notch (see Figs. 4–6), fracture preferentially initiates from this area and then propagates into the specimen. Two questions are examined in some detail:

- (1) The point on the inner surface of the specimen at which fracture may initiate.
- (2) The direction of crack propagate.

Following the assumption that crack extension starts in the plane normal to the direction of greatest tensile stress (the maximum tensile stress criterion; see, for example, Erdogan and Sih, 1963 and Otsuka et al., 1975), assume that the specimen fractures from the point and in the direction where the tensile stress first reaches a critical value  $\sigma_c$ ; this is similar to the maximum tensile-stress criterion. This critical tensile stress,  $\sigma_c$ , is associated with the energy required for breaking the interatomic bonds in the direction of maximum tension. The quantity  $\sigma_c$  may be related to other fracture measures such as  $K_{Ic}$  or

$G_c$ . For isotropic materials, these measures are not direction-dependent, whereas in the anisotropic case, they are, i.e. different planes require different energies to fracture (see Table 1). Thus the role of the surface energies of different cleavage planes should be taken into consideration.

The fracture resistance (or surface energy) of sapphire for different crystallographic planes is given in Table 1. Fig. 6 shows a typical point  $P$  on the notch surface. A typical cleavage plane passing through this point is denoted by  $mm$  (making the angle  $\alpha$  with respect to the  $x$ -axis). Using the FEM results for points on the inner surface of the notch, the tensile stress,  $\sigma_{nn}$ , on the cleavage plane,  $mm$ , is obtained from  $\sigma_{nn} = (\sigma_{yy} - \sigma_{xx})\cos^2\alpha + \sigma_{xx} - \sigma_{xy}\cos 2\alpha$ . This tensile stress,  $\sigma_{nn}$ , has the tendency to break the interatomic bonds along the  $mm$ -direction. Finally, for each cleavage plane, the point at which the tensile stress,  $\sigma_{nn}$ , is maximum is found. The location of this point on the semi-circle of the notch is denoted by angle  $\beta^{(S)}$ ; see Fig. 6. It should be mentioned that even though at this point  $\sigma_{nn}$  is maximum on the cleavage plane  $mm$ , this cleavage plane is not necessarily shear-free. All 48 distinct nodes on the notch are examined. At each node the existing 6 different cleavage planes are studied (Fig. 2). Therefore, for each specimen,  $\sigma_{nn}$  is calculated for  $48 \times 6 = 288$  different cases.

In general, a cleavage plane makes an angle  $\lambda$  with the  $(11\bar{2}0)$ -plane. The  $mm$ -direction represents the intersection of the corresponding cleavage plane with the  $(11\bar{2}0)$ -plane. Therefore,  $\sigma_{nn}$  does not necessarily represent the tensile stress acting normal to the actual cleavage plane. For a plane-stress condition, the tensile stress acting on the actual cleavage plane is  $(\sin^2\lambda)\sigma_{nn}$ . This is used in the corresponding calculations.

According to the procedure discussed above, the related calculations are carried out for all 6 specimens; see Fig. 3. The results are shown in Table 2. In Table 2,  $\beta^{(S)}$  defines the point on the notch surface at which the calculated  $\sigma_{nn}$  is maximum on the particular cleavage plane of angle  $\alpha$ . The angle  $\beta^{(S)}$  (the angular position of the point of maximum  $\sigma_{nn}$  on the notch surface) is positive when measured from the  $x$ -axis in the clock-wise direction. The experimental counterpart of  $\beta^{(S)}$  is denoted by  $\beta_{(F)}$ ; this is the angle at which the fracture was actually

Table 2

Comparison of FEM and experimental results; (S), (G) and (F) stand for tensile-stress, energy-release-rate and fractured-by-experiment, respectively (see Figs. 2, 3, and 6)

Crystallographic planes	Angles (°)	Specimen #1	Specimen #2	Specimen #3	Specimen #4	Specimen #5	Specimen #6
(10 $\bar{1}$ 0)	$\alpha$	90	180	32.4	<b>122.4*</b>	52	142
	$\beta^{(S)}$	93.7	22.5	142.5	<b>60</b>	127.5	56.2
	$\beta^{(G)}$	93.7	30	142.5	<b>60</b>	127.5	63.7
(1 $\bar{1}$ 02)	$\alpha$	<b>57.6*</b>	147.6	0	90	19.6	<b>109.6*</b>
	$\beta^{(S)}$	<b>112.5</b>	41.2	157.7	93.7	142.5	<b>71.2</b>
	$\beta^{(G)}$	101.2	48.7	157.7	86.2	138.7	<b>71.2</b>
(10 $\bar{1}$ 2), (0 $\bar{1}$ 12), (1 $\bar{2}$ 16), (2 $\bar{1}$ 16)	$\alpha$	38	128	–19.6	70.4	0	90
	$\beta^{(S)}$	123.7	67.5	41.2	112.5	153.7	82.5
	$\beta^{(G)}$	112.5	67.5	48.7	112.5	142.5	78.7
(0001), (11 $\bar{2}$ 6), ( $\bar{1}$ 126)	$\alpha$	0	90	–57.6	32.4	–38	52
	$\beta^{(S)}$	18.7	90	63.7	131.2	45	127.5
	$\beta^{(G)}$	22.5	86.2	67.5	127.5	45	116.2
(10 $\bar{1}$ 2), (0 $\bar{1}$ 12), (2 $\bar{1}$ 16), (1 $\bar{2}$ 16)	$\alpha$	–38	52	–95.6	–5.6	–76	14
	$\beta^{(S)}$	45	112.5	86.2	33.7	67.5	146.2
	$\beta^{(G)}$	60	101.2	78.7	33.7	67.5	142.5
(1 $\bar{1}$ 02)	$\alpha$	–57.6	32.4	<b>–115*</b>	–25.2	<b>–95.6*</b>	–5.6
	$\beta^{(S)}$	71.2	127.5	<b>116.2</b>	41.2	<b>101.2</b>	33.7
	$\beta^{(G)}$	78.7	112.5	90	45	105	37.5
Experimental results	$\alpha_{(F)}$	61, 53	126, 135	–116, –110	115, 83	–99, –97	112, 99
	$\beta_{(F)}$	115, 120	70, 74	120, 115	63, 65	101, 100	63, 68

initiated on the notched specimen. The values of this angle for different specimens are also presented in Table 2.

#### 4.2. Calculation of energy-release rate due to cracking of the notch surface

Assume, now, that a crack with length  $L$  occurs in the direction  $mm$ , shown in Fig. 6. This changes the total potential energy of the sample. Denote by  $G^{(mm)}$  this energy change due to cracking. In what follows, it is assumed that the crack length (in any direction) is always  $L$  ( $L \approx 50 \mu\text{m}$ ). Thus, the term ‘energy released per  $L$  crack length’ will be replaced by the commonly used term ‘energy-release rate’, using  $L$  as the unit of length. To calculate  $G^{(mm)}$ , find the difference between the work done by the externally applied loads for the two cases of the un-cracked and cracked specimen. For the un-cracked

specimen, the calculation of the energy is straightforward (use the FEM mesh given in Fig. 5), whereas for the cracked specimen, the calculation requires a new FEM mesh to account for the crack. For this, fine discretization is added around the point where the crack is placed; see Fig. 7.

As Fig. 8 (this is a magnified Fig. 7) shows, this mesh can simulate cracks along 7 different directions and this provides the possibility to approximately locate one of these 7 directions on the cleavage plane,  $mm$ . As a result, the use of this mesh facilitates the examination of all 6 different cleavage planes (Fig. 2) at any typical point on the notch surface. Then, for the examination of points on the notch surface, the fine mesh is located at all 48 nodes along the notch surface, as shown in Fig. 7. In addition, Fig. 8 demonstrates the configuration of the points around the fine mesh before and after crack opening.

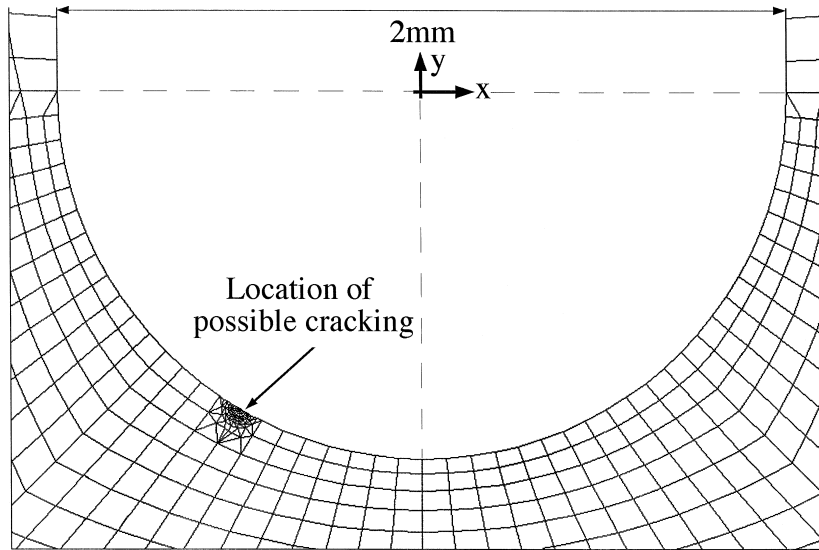


Fig. 7. FEM mesh for the notched throat at a location of possible cracking.

A calculation similar to the one performed for tensile stress is performed to find the point at which the maximum energy would be released if a crack

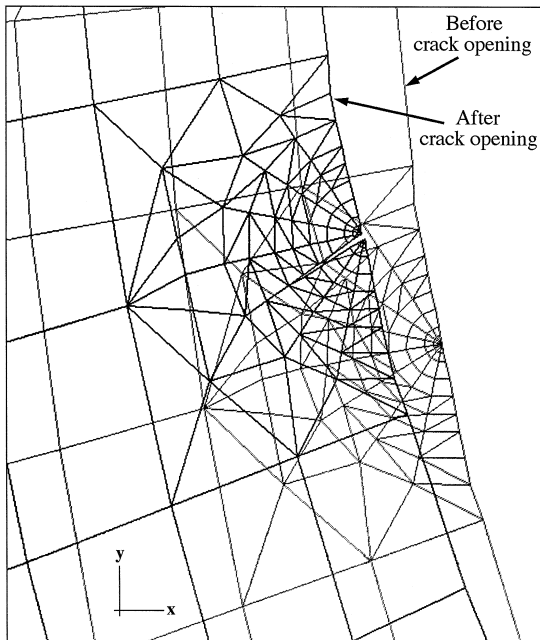


Fig. 8. FEM mesh illustrating the configurations before and after crack-opening.

occurs at that point and in one particular cleavage plane. Note that, for each specimen, calculation of the tensile stress requires just one run of ABAQUS, whereas the energy-release-rate calculation involves  $48 \times 6 = 288$  runs of ABAQUS. The released energy due to the occurrence of a crack in the  $mm$ -direction,  $G^{(mm)}$ , is calculated by the following formula:

$$G^{(mm)} = \sum_{i=1}^M \left\{ P_i^{(x)} [u_i^{(c)} - u_i^{(nc)}] + P_i^{(y)} [v_i^{(c)} - v_i^{(nc)}] \right\}, \quad (1)$$

where  $P_i^{(x)}$  and  $P_i^{(y)}$  are the  $x$ - and  $y$ -components of an externally applied point force at the corresponding  $i$ th point, respectively;  $u_i^{(c)}$  and  $v_i^{(c)}$  are the displacements of the  $i$ th point of a *cracked* notch in the  $x$ - and  $y$ -directions, respectively;  $u_i^{(nc)}$  and  $v_i^{(nc)}$  are the displacements of the  $i$ th point of a *non-cracked* notch in the  $x$ - and  $y$ -directions, respectively and, finally,  $M$  is the number of the externally applied point forces. Moreover, as mentioned earlier, the magnitude of the resultant load associated with  $P_i^{(x)}$  and  $P_i^{(y)}$  is immaterial. The calculated values of  $u_i^{(nc)}$  and  $v_i^{(nc)}$  are not too sensitive to the fineness of the mesh around the crack tip, because the crack and the points where  $u_i^{(nc)}$  and  $v_i^{(nc)}$  are calculated

(the points where the external loads are considered, Fig. 6) are far from each other.

According to the procedure discussed above, for each specimen and for each of the 6 directions shown in Fig. 2, denoted by  $\alpha$  in Fig. 6, ABAQUS is run 48 times, corresponding to 48 nodal points on the notch surface. Then  $G^{(mm)}$  is calculated for all these 48 different configurations. The maximum,  $G_{\max}$ , of this set of 48  $G^{(mm)}$ 's occurs at a point on the notch surface,  $G_{\max}$ , denoted by  $\beta^{(G)}$ ; see Fig. 6 and Table 2. The angle  $\beta^{(G)}$  (the angular position on the semi-circular notch) at which  $G_{\max}$  occurs is positive when measured from the  $x$ -axis in the clock-wise direction. Note that  $\beta^{(G)}$  defines the point on the notch surface where the maximum energy is released if a crack initiates in the cleavage plane of direction  $\alpha$  shown in Fig. 6. Since there are 6 different  $\alpha$  directions,  $\beta^{(G)}$  is calculated 6 times for each specimen. The results are shown in each column of Table 2.

Finally, the variations of the normal tensile stress,  $\sigma_{nn}$ , and the energy released,  $G^{(mm)}$ , with respect to the location on the notch-surface are presented in Fig. 9 for specimen #1 and the cleavage plane #5 ( $\alpha = -38^\circ$ ). This figure shows that the  $\sigma_{nn}$ - and  $G^{(mm)}$ -curves have: (1) fairly sharp maxima; (2) similar trend and (3) their maximum points occur at different angles. The first result is important from the experimental viewpoint, since the points of maxi-

mum  $\sigma_{nn}$  and  $G^{(mm)}$  are distinct and can easily be compared with the actual failure location.

## 5. Results and discussion

The results of the numerical analysis of the two fracture measures (tensile stress and energy-release rate) are presented in Table 2. The point and the direction of fracture ( $\beta_{(F)}$  and  $\alpha_{(F)}$ ) are directly measured on the fractured specimens (Fig. 10 shows the picture of 6 of the broken specimens). The Laue-diffraction analysis is performed on two of the specimens and the crystallographic indices are determined. This determination along with the geometric considerations of the crystallographic planes, facilitate the determination of the crystallographic indices of all other planes. The experiments are conducted on 2 specimens of each configuration shown in Fig. 3 and, thus, altogether, 12 specimens are used. Table 2 is a summary of the FEM analysis as well as the experimental results on all 6 different specimens. In each column of Table 2, the bold-face numbers and the numbers with a superscript star indicate that the corresponding FEM results match the experimental results. Note that the FEM analysis is performed on 48 distinct points on the notch surface, and thus every two consecutive points are about  $180^\circ/48 \approx 4^\circ$  apart. In view of this, the FEM results such as the values of  $\alpha$ ,  $\beta^{(S)}$ , and  $\beta^{(G)}$ , are accurate to within  $\pm 4^\circ$ . Next, the conclusions drawn from Table 2 are presented.

Let us now compare the experimental and numerical results from Table 2; this is done by comparing  $\alpha$ 's and  $\alpha_{(F)}$ 's and also  $\beta$ 's and  $\beta_{(F)}$ 's. In order to clarify how this comparison is made, consider the column corresponding to the specimen #1 in Table 2. As is seen, the cleavage plane ( $1\bar{1}02$ ) is the only plane whose corresponding numerical results (angles  $\alpha$  and  $\beta^{(S)}$ ) match closely with the experimental results (angles  $\alpha_{(F)}$  and  $\beta_{(F)}$ ); note that  $\alpha$ 's indicate the cleavage plane and  $\beta$ 's are the angular positions of the points on the notch surface (Fig. 6). This shows that specimen #1 is fractured along the ( $1\bar{1}02$ )-plane at the point (on the notch surface) where the tensile stress is maximum.

This method of comparison shows that 5 of the specimens are fractured along the weakest cleavage family of planes  $\{1012\}$  and one specimen (#4) is

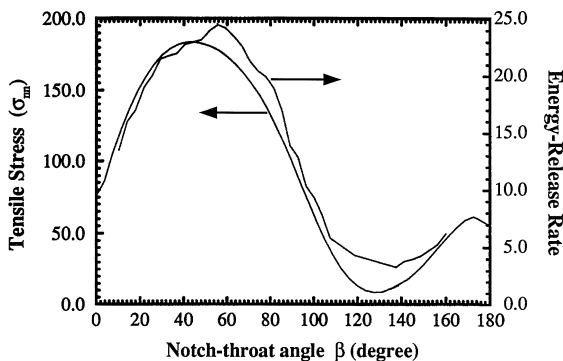


Fig. 9. Tensile stress and energy-release rate versus notch-throat angle  $\beta$  for specimen #1 and cleavage plane #5 ( $\alpha = -38^\circ$ ); see Figs. 2 and 6.

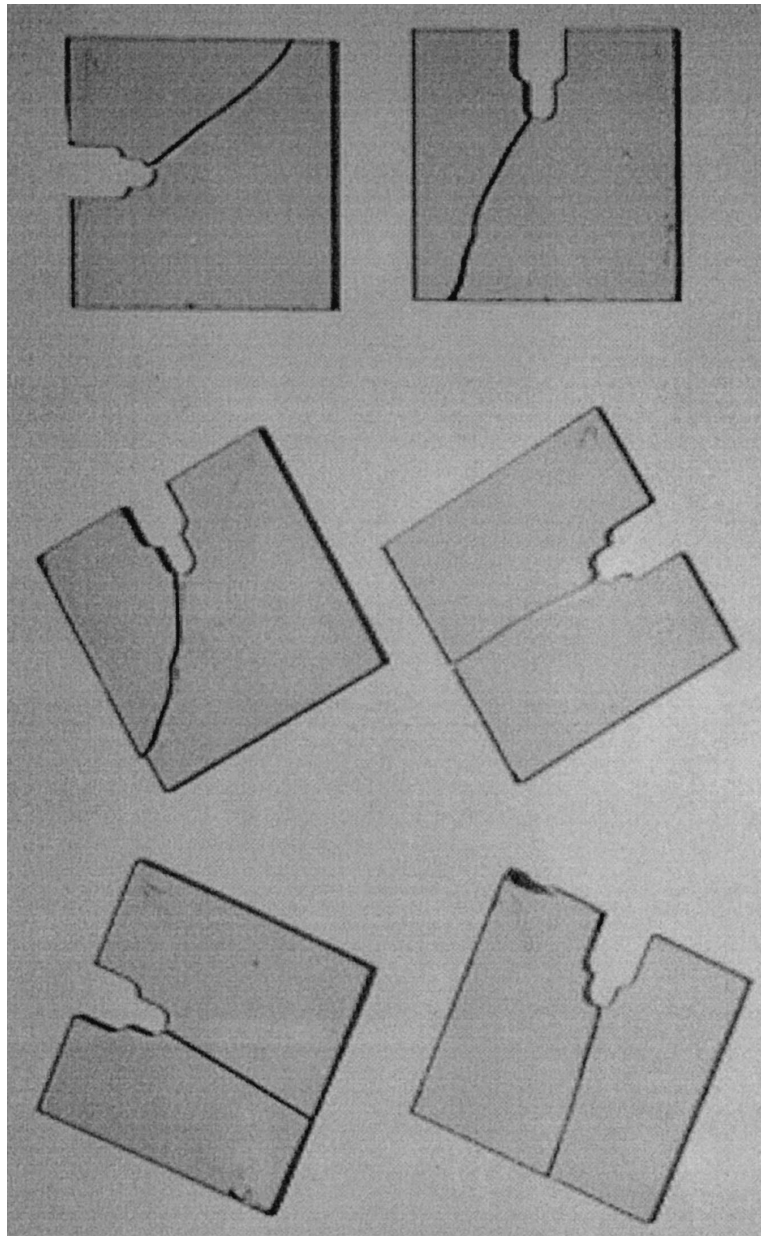


Fig. 10. Fractured specimens; compare with Fig. 3.

fractured along the second weakest family of cleavage planes  $\{10\bar{1}0\}$ ; see Table 1. Moreover, Table 2 shows that 5 out of 6 samples (except for #2) are fractured according to the *maximum-tensile stress* ( $\beta^{(S)}$  in bold). For some of the samples (#4 and #6) the FEM results show that the maximum

tensile-stress and maximum energy-release rate criteria predict the same crack path. These occasional agreements between the predictions made by the stress- and energy-based criteria are also observed in the analytical studies; see Azhdari and Nemat-Nasser (1996b).

The FEM analysis shows that fracture occurs in the direction where a *high tensile stress acts on a weak cleavage plane*. In other words, it is a compromise between the surface energy (the lower, the easier to fracture) and the tensile stress acting normal to this surface (the higher, the more probable to break the interatomic bonds). Furthermore, wherever a combination of these two is optimized, fracture occurs. For example, there are cases where the tensile stress acting on the basal plane (0001) (the strongest cleavage plane) is much higher than the one acting on the family of  $\{\bar{1}012\}$ -planes, but fracture occurs on the  $\{\bar{1}012\}$  ones. This is also observed when the criterion of the energy-release rate is studied. This study highlights the role of the cleavage planes and the differences between their surface energies in the fracturing of single crystals.

Note that in a brittle single crystal, it is very unlikely that a crack (or a micro-crack) would initiate and propagate according to the maximum- $K_I$  (zero- $K_{II}$ ) fracture criterion. This is because a weak cleavage plane does not always happen to be in the direction of the maximum- $K_I$  (or equivalently, zero- $K_{II}$ ). This comment applies to the case of an already-cracked body. For the case of a notched specimen, fracturing does not always occur in the direction where the tensile stress is maximum, because the plane in the direction of the maximum tensile stress may be a relatively strong cleavage plane. Note that the strength of a certain plane in a brittle solid is expected to depend on the Young modulus  $E$  and the surface energy  $\gamma$ . Thus, the product ( $E\gamma$ ) may be considered as a measure of the strength of a plane against fracture.

### 5.1. Potential fracture criteria

Now, consider a fracture criterion which is based upon a combination of the strength of the cleavage plane and the tensile stress acting on that plane. Examine the ratio  $A = \sigma_{nn}/(E_{nn}\gamma_\alpha)$  and assume that *fracture initiates at the point and in the direction where the ratio  $A = \sigma_{nn}/(E_{nn}\gamma_\alpha)$  is maximum*. Here,  $nn$  is normal to the direction of the cleavage plane on which crack propagation may occur,  $\sigma_{nn}$  is the tensile stress acting normal to that plane, and  $\gamma_\alpha$  is the surface energy of that cleavage plane. In order to make this ratio dimensionless, consider the square

root of the strength term and also use a characteristic length, e.g. the notch radius  $R_0$ . The result is

$$A^{(N)} = \sqrt{2\pi R_0} \frac{\sigma_{nn}}{\sqrt{\gamma_\alpha E_{nn}}}, \quad (2)$$

where the superscript (N) stands for ‘notch’. Note the similarity between the  $A^{(N)}$ -criterion and the energy formula of Griffith (1921, 1925)  $\sigma_c = \sqrt{E\gamma}/\sqrt{\pi a}$ , where  $\sigma_c$  is the critical stress for the extension of a pre-existing crack of length  $a$ .

In order to verify the validity of the  $A^{(N)}$ -fracture criterion, the FEM results for the stresses,  $\sigma_{nn}$ , the values of the corresponding  $\gamma_\alpha$ 's from Table 1, and  $E_{nn}$  obtained from the elastic constants given in Section 3.1 are used. The results are interesting in the sense that the predictions made by the criterion of the maximum- $A^{(N)}$  match the experimental results. The point and the direction of fracturing of 5 specimens are predicted by this fracture criterion, i.e. for 5 specimens (from 2), when the 6 different cleavage planes are compared using criterion (2), it is observed that the maximum- $A^{(N)}$  fracture criterion identifies the ‘cleavage planes’ along which the specimens fractured in the actual tests.

In contrast to the criterion of maximum- $A^{(N)}$ , the criterion of maximum- $G^{(mm)}/\gamma_\alpha$  fails to predict the fracturing of any of the 6 specimens. Therefore, the FEM results and the experiments conducted on these 6 different specimens show that the maximum- $A^{(N)}$  criterion is capable of predicting the fracture phenomenon of such notched specimens. Note that this criterion is basically a stress-based fracture criterion, although it contains the parameter  $\gamma_\alpha$  which is an energy-related parameter. Summing up, this criterion can be justified if it is interpreted as follows: The maximum- $A^{(N)}$  may be a suitable fracture criterion because it is based upon the local tensile stress derived from the global external loading and also it contains an energy term which represents the energy required to break the atomic bonds over the fracture plane.

### 5.2. Comments on the fracture criterion

The criterion of maximum- $A^{(N)}$  is defined for a notched body. Consider applying this criterion to a cracked body to predict possible crack kinking. For a

notched body, the normal stress  $\sigma_{nn}$  is finite, whereas if the notch is shrunk to a sharp crack, then this stress becomes infinite at the crack tip (singular stress). Define the hoop stress intensity factor,  $K_{nn}$ , through  $\sigma_{nn} = K_{nn}/\sqrt{2\pi r}$ , where  $r$  measures the distance from the crack tip. Substitute this for  $\sigma_{nn}$  into (2) and let  $r$  be equal to  $R_0$ . Then, the characteristic length  $R_0$  cancels out and we obtain

$$A^{(C)} = \frac{K_{nn}}{\sqrt{\gamma_\alpha E_{nn}}}, \quad (3)$$

where the superscript (C) stands for ‘crack’. Now, consider the condition for crack kinking in single crystals of brittle solids having a finite number of cleavage planes, as follows: *Among all cleavage planes passing through the tip of a pre-existing crack, crack extension occurs on the cleavage plane which renders  $A^{(C)}$  maximum.* This can be reworded as follows: *A pre-existing crack kinks along a cleavage plane on which  $A^{(C)}$  is maximum.* Note that, according to the stress-based fracture criteria of maximum- $A^{(N)}$  or maximum- $A^{(C)}$ , fracture most likely occurs on cleavage planes which carry non-zero shear stresses. This is not in accordance with the hoop and shear stress intensity factor (HSIF and SSIF) criteria where the maximum-HSIF is accompanied by the zero-SSIF, as discussed by Azhdari and Nemat-Nasser (1996a) who, however, do not address the anisotropy stemming from the material resistance to fracturing.

A related criterion for the crack extension direction in orthotropic composite materials is proposed by Buczek and Herakovich (1985). They suggest that a crack kinks in the  $\phi$ -direction if the ratio  $R(r_0, \phi) = \sigma_{\phi\phi}(r_0, \phi)/T_{\phi\phi}(\phi)$  is maximum, where  $\sigma_{\phi\phi}$  is the stress normal to the  $\phi$ -direction,  $T_{\phi\phi}$  is the tensile strength of the composite in the  $\phi$ -direction and  $r_0$  is a given distance from the crack tip (to be determined experimentally from a baseline test). Note that a drawback of this criterion is its dependence on the experimental determination of  $r_0$ . The fracture criterion in Eq. (3) has no dependency on distance from the crack tip.

Based on the maximum- $A^{(C)}$  criterion, we seek to modify the commonly used energy-release rate criterion so as to account for the multi-valuedness of the

surface-energy function, i.e. we consider a criterion similar to Eq. (3) for the energy-release rate for an anisotropic solid having multiple cleavage planes. First, consider the energy-release rate formula (Irwin’s equation)

$$G = \frac{C'_{11}}{2} [f_1(\mu, \omega) K_I^{(k)} K_I^{(k)} + f_2(\mu, \omega) K_{II}^{(k)} K_{II}^{(k)} + f_3(\mu, \omega) K_I^{(k)} K_{II}^{(k)}], \quad (4)$$

where  $f_i$ ’s are known functions of the kink angle  $\omega$  and  $\mu$  ( $\mu$  stands for ‘material parameters’, i.e. functions of material constants  $C_{ij}$ ’s in Section 3.1),  $K_I^{(k)}$  and  $K_{II}^{(k)}$  are the stress intensity factors at the tip of the vanishingly small kink of angle  $\omega$  with respect to the pre-existing crack direction and  $C'_{11}$  is the compliance in the kink direction; see also Azhdari and Nemat-Nasser (1996b). When the driving force (the external loading expressed by  $K_I^{(k)}$  and  $K_{II}^{(k)}$ ) reaches the value where the energy-release rate is equal to the surface energy of the cleavage plane lying in the  $\omega$ -direction, then fracturing of this cleavage plane takes place and one has  $G = \gamma_\omega$ . If we seek to find the kink angle  $\omega$  by maximizing the function on the right-hand side of Eq. (4), the resulting kink angle may lie on a strong cleavage plane which does not fracture under the applied loads and therefore does not define a physically meaningful kink angle. An alternative to this criterion is to include in the right-hand side the surface energy of the material corresponding to the  $\omega$ -plane and define

$$B^{(C)} = \frac{C'_{11}}{2\gamma_\omega} [f_1(\mu, \omega) K_I^{(k)} K_I^{(k)} + f_2(\mu, \omega) K_{II}^{(k)} K_{II}^{(k)} + f_3(\mu, \omega) K_I^{(k)} K_{II}^{(k)}], \quad (5)$$

where  $B^{(C)}$  is a dimensionless quantity and, again, the superscript (C) stands for ‘crack’.

Maximizing, now,  $B^{(C)}$  with respect to  $\omega$  may give the angle at which the pre-existing crack kinks (the occurrence of this kink releases energy at the rate of  $\gamma_\omega$ ). Note that: (1) the criterion of the maximum- $B^{(C)}$  is suitable for the case when the surface energy  $\gamma_\omega$  is a function of angle  $\omega$  (an anisotropic

quantity) and (2) the maximum- $A^{(C)}$  criterion deals with quantities prior to kinking such as the HSIF ( $K_{nn}$ ), whereas the maximum- $B^{(C)}$  criterion involves quantities at the tip of a kinked crack, e.g.  $K_I^{(k)}$  and  $K_{II}^{(k)}$ .

## 6. Summary and conclusions

The fracture of homogeneous, linearly elastic and anisotropic solids is considered. Sapphire, a single-crystal and highly brittle material, is selected for the experiments. Notched specimens with six different orientations, Figs. 2 and 3, are made from a sheet of sapphire with the crystallographic orientation  $(11\bar{2}0)$ . Specimens are loaded (and eventually fractured) by heating up a piece of steel block placed inside the notch; see Fig. 4. Two parameters are measured after each test: the location of the point on the inner surface of the notch at which fracture is initiated and the direction in which the crack propagates. Laue-diffraction analysis is used to verify the crystallographic indices of the fractured surfaces. The FEM code ABAQUS is employed to simulate the loading process of the specimens. Table 2 is a summary of the numerical as well as the experimental results. Assuming that the elastic–stiffness constants and the surface energies of different cleavage planes reported in the literature for sapphire (and used here in the numerical simulations) are reasonably accurate, the following conclusions are obtained:

(1) For the *notched* specimens, fracture occurs in the direction where a high tensile stress acts upon a weak cleavage plane. In other words, there is an interplay between the surface energy (the lower, the easier to fracture) and the tensile stress acting normal to this surface (the higher, the greater chance of breaking the interatomic bonds).

(2) The tensile-stress criterion is compared with the released-energy criterion. It is observed that almost all of the notched specimens are fractured where the tensile stress on a weak cleavage plane is maximum. In general, the energy criterion failed to predict the observed fracture direction.

(3) The maximum- $K_I$  (zero- $K_{II}$ ) or the maximum- $G$  fracture criterion does not seem to apply to single-crystal brittle solids where there is a finite number of cleavage planes.

(4) In view of (1), the fracture criterion of maximum  $A^{(N)} = \sqrt{2\pi R_0} \sigma_{nn} / \sqrt{\gamma_\alpha E_{nn}}$  is proposed. The predictions made by this criterion matched the experimental results for 5 out of 6 specimens.

(5) The stress-based fracture criterion appears to better predict the fracturing of single-crystal brittle solids. This may also be applied to predict *crack kinking*.

(6) A crack in a brittle single crystal kinks in the direction where  $A^{(C)} = K_{nn} / \sqrt{\gamma_\alpha E_{nn}}$  is maximum. Here,  $K_{nn}$  is the hoop stress intensity factor normal to a cleavage plane located in the  $n$ -direction and  $\gamma_\alpha$  is the surface energy of that cleavage plane. Note that, the cleavage plane (equivalently, the  $n$ -direction) which renders  $A^{(C)} = K_{nn} / \sqrt{\gamma_\alpha E_{nn}}$  maximum may not, in general, be the zero-shear plane. This is not in accordance with the maximum-hoop (zero-shear) stress intensity factor; see Azhdari and Nemat-Nasser (1996a).

(7) For the notched sapphire specimens, Laue-diffraction analysis, along with the considerations of the geometry of the unit cell of sapphire, shows that the two weakest families of cleavage planes,  $\{\bar{1}012\}$  and  $\{10\bar{1}0\}$ , happen to be the fractured planes. This study highlights the role of the cleavage planes and the differences between their surface energies in the fracturing of single crystals.

(8) The commonly used energy-release-rate fracture criterion is modified such that it can be used for a cracked single crystal which possesses a finite number of cleavage planes; see Eq. (5).

While experiments on only 12 specimens may not be sufficient to support the above conclusions, these conclusions appear to be reasonable on physical grounds and they should provide guidance for future work in this area.

## Acknowledgements

This work has been supported in part by ARO under Grant No. DAAL03-92-K-0002 and in part by the Institute for Mechanics and Materials (IMM) at the University of California, San Diego. Thanks are due to Dr. M. Beizai who helped to develop the graphs of the paper. The computations reported here were carried out on a CRAY-C90 at the San Diego Supercomputer Center.

## References

- Azhdari, A., 1995. *Fracturing in Anisotropic Brittle Solids*. Ph.D. dissertation. University of California, San Diego.
- Azhdari, A., Nemat-Nasser, S., 1996a. Hoop stress intensity factor and crack kinking in anisotropic brittle solids. *Int. J. Solids Struct.* 33, 2033–2037.
- Azhdari, A., Nemat-Nasser, S., 1996b. Energy-release rate and crack kinking in anisotropic brittle solids. *J. Mech. Phys. Solids* 44, 929–951.
- Buczek, M.B., Herakovich, C.T., 1985. A normal stress criterion for crack extension direction in orthotropic composite materials. *J. Composite Mater.* 19, 544–548.
- Erdogan, F., Sih, G.C., 1963. On the crack extension in plates under plane loading and transverse shear. *J. Basic Eng.* 85, 519–527.
- Gilman, J.J., 1960. Direct measurements of the surface energies of crystals. *J. Appl. Phys.* 31, 2208–2218.
- Griffith, A.A., 1921. The phenomenon of rupture and flow in solids. *Philos. Trans. R. Soc. Ser. A*: 221, 163–198.
- Griffith, A.A., 1925. The theory of rupture. In: Biezeno, Burgers (Eds.), *Proc. 1st Int. Congr. Appl. Mech.* Waltman, Delft, pp. 55–63.
- Obata, M., Nemat-Nasser, S., Goto, Y., 1989. Branched cracks in anisotropic elastic solids. *J. Appl. Mech.* 56, 858–864.
- Otsuka, A., Mori, K., Miyata, T., 1975. The condition of fatigue crack growth in mixed mode condition. *Eng. Fract. Mech.* 7, 429–439.
- Sih, G.C., 1972. A special theory of crack propagation, method of analysis and solution to crack problems. In: Sih, G.C. (Ed.), *Mechanics of Fracture*, vol. 1. Noordhoff, Leyden.
- Tsai, S.W., Wu, E.M., 1971. A general theory of strength for anisotropic materials. *J. Composite Mater.* 5, 58–81.
- Wachtman, J.B., Tefft, W.E., Lam, D.G., Stinchfield, R.P., 1960. Elastic constants of synthetic single crystal corundum at room temperature. *J. Natl. Bureau Standards* 64A (3), 213–228.
- Wiederhorn, S.M., 1969. Fracture of sapphire. *J. Am. Ceram. Soc.* 52 (9), 485–491.
- Wu, E.M., 1974. In: Broutman, L.J. (Ed.), *Strength and Fracture of Composites in Composite Materials*, vol. 5. Academic Press, New York, pp. 191–247.